IET Control Theory & Applications

Research Article

IET Journals
The Institution of Engineering and Technology

Output feedback-based sliding mode control for disturbed motion control systems via a higher-order ESO approach

ISSN 1751-8644
Received on 11th January 2018
Revised 18th April 2018
Accepted on 11th July 2018
E-First on 31st July 2018
doi: 10.1049/iet-cta.2018.5197
www.ietdl.org

Jianliang Mao[1], Jun Yang[1], Shihua Li[1] ✉, Yunda Yan[1], Qi Li[1]

[1]*Key Laboratory of Measurement and Control of Complex Systems of Engineering, Ministry of Education, School of Automation, Southeast University, Nanjing, Jiangsu 210096, People's Republic of China*

✉ *E-mail: lsh@seu.edu.cn*

Abstract: This study presents an output feedback-based sliding mode control approach for motion control systems with mismatched/matched disturbances. The key idea of this study is to reconstruct the unmeasured auxiliary states and disturbances synchronously online by constructing a higher-order extended state observer (HOESO). It is shown that the resulting sliding mode controller based on HOESO can drive the system output to an ultimately bounded region, which can be regulated arbitrarily small by assigning a sufficiently large scaling gain. Different from the existing extended state observer methods, the newly proposed HOESO treats the known dynamics satisfying the Lipschitz condition and the unknown higher-order disturbances separately. As such, it provides a feasible way for higher-precision states/disturbance estimation. Thanks to the utilisation of HOESO, the upper bound of disturbances is not necessarily required as a priori and the switching gain is adaptively chosen based on the estimation error such that the chattering effects can be significantly reduced. Experiments for speed regulation of a brushless DC motor are conducted to verify the effectiveness of the proposed method.

1 Introduction

During the past decades, many advanced control theories have been raised for a family of non-linear high-order systems with mismatched/matched disturbances [1–5]. Among these methods, sliding mode control (SMC) receives a great deal of attention in industrial applications, due to its powerful robustness against plant uncertainties and external disturbances [6–8]. To date, most of the existing results on SMC design paid attentions to the matched disturbances rejection. However, for many practical motion control systems such as brushless DC (BLDC) drives [9], electro-hydraulic systems [10, 11], permanent magnet synchronous motor [12], and MAGnetic LEViation suspension system [13, 14], the so-called matching condition is not satisfied because the external disturbances usually enter the system via different channels from the control input. Robustness against the mismatched disturbances by means of SMC approach has always been a challenging issue.

To eliminate the side effects caused by mismatched disturbances, numerous original SMC methods are put forward from different aspects in recent years, such as integral-based approach [15, 16], linear matrix inequality-based approach [17], invariant ellipsoid approach [18], and disturbance observer (DOB)-based approach [14, 19]. Nevertheless, these results are only applicable to the case when all the plant states are physically measurable. In practice, for a variety of reasons, e.g. the restrictions of mechanical assembly and manufacturing costs, only a few states are available in many applications [20], which motivates the research on the SMC design via output feedback. In general, the existing output feedback-based SMC methods (see [21–27] and references therein) can be classified into the following two strategies.

The first strategy is referred to the direct output-based SMC design without constructing an explicit state observer. It mainly focuses on the sliding surface design depending upon directly output signals or indirectly a dynamic compensator that only relies on the outputs [21–24]. However, this kind of approach generally raises rather restrictive requirements on the model structure of system. For instance, the product of system output and input matrices should satisfy the full-rank condition. Additionally, the mismatched disturbances considered are generally supposed to be H_2 norm-bounded. These assumptions will inevitably impose restrictions on motion control applications [14].

Another strategy can be summarised as the observer-based SMC approach. The underlying idea here is quite intuitive, i.e. a state observer/estimator, e.g. high-gain observer [25] or sliding mode observer [26, 27] is developed to reconstruct all the unmeasurable states by means of the input and output signals of system. These estimates are then utilised for the output-feedback based SMC design. However, in order to reject the bounded equivalent input disturbances, most of the existing results (see [25, 26] and references therein) exhibit high-frequency switching with large control gains, which leads to the serious chattering phenomenon inevitably. To eliminate the undesired chattering, the boundary layer method is generally employed but causes the performance degradation on disturbance rejection. Recently, it has been extensively reported that the DOB technique can be utilised as an alternative way for chattering attenuation [14, 28, 29].

Among various disturbance estimation methods, the extended state observer (ESO) [30] provides an adequate approach assisting the output feedback control design as it can be utilised to estimate the states as well as the lumped disturbances synchronously [10, 31–33]. The application of ESO to alleviate chattering of SMC can be found in [28, 29, 34]. However, as pointed out by Godbole *et al.* [35], the standard ESO can only achieve the desired estimation accuracy of slow time-varying or constant disturbances, which is not suitable for the case when higher precision is required. Furthermore, under the framework of standard ESO, the rest dynamics except for integral chain ones, no matter known or unknown, are lumped together for estimation [13, 35–37]. Such a straightforward treatment has largely facilitated controller design, but will definitely cause the following two drawbacks. First, the known dynamics in many practical systems should have great impacts on control performance. It would be beneficial to fully take advantage of these system dynamics for the controller design. Second, these known dynamics shall be very large during the transient process. To obtain the satisfactory control performance, the observer gains of the standard ESO are generally tuned large enough, which leads to the adverse impacts such as the peaking phenomenon and the noise amplification.

Given the aforementioned facts, an output feedback-based SMC approach incorporating a newly developed higher-order ESO

(HOESO) is proposed for the disturbed motion control systems. Under the presented framework, the unmeasured auxiliary states and disturbances are reconstructed synchronously online, which are further utilised for the development of the sliding mode controller. It is shown that the system output is rendered ultimately bounded even in the presence of mismatched time-varying disturbances. Furthermore, the ultimate boundary can be made arbitrarily small by assigning a tunable scaling gain. To demonstrate the effectiveness of the proposed method, experiments on a BLDCM drive system provided by Texas Instruments are conducted. The major contributions of this paper are summarised as follows:

(1) As compared to the existing ESO, the newly designed HOESO is capable of estimating higher-order disturbances. Different from the results in [35, 36], the proposed observer handles the known dynamics satisfying the Lipschitz condition and the unknown higher-order disturbances separately, which guarantees a higher observation accuracy with the same observer gains.
(2) Thanks to the utilisation of the HOESO, in comparison with the results in [25, 26], the upper bound of the time-varying disturbances is not necessary to be known as a priori. Moreover, the chattering effects can be significantly reduced since the switching gain is adaptively chosen based on the estimation error.

The remaininf of this paper is organised as follows. Section 2 states the problem. Section 3 presents the design details of the newly proposed HOESO-based SMC approach. An application to a BLDCM drive system is given in Section 4. Section 5 concludes this paper.

2 Problem formulation

Consider the second-order benchmark model of an industrial BLDCM drive system as follows [9]:

$$\begin{cases} \dot{\omega}(t) = \dfrac{1}{J_m}[-b_c\omega(t) + 2k_t i_a(t) - \tau_{\mathrm{d}}(t)], \\ \dot{i}_a(t) = \dfrac{1}{L_a}\left[-k_v\omega(t) - R_a i_a(t) + \dfrac{1}{2}V_a u(t)\right] \end{cases} \tag{1}$$

where $u(t)$ is the inverter duty ratio (system input), $\omega(t)$ is the angular velocity (system output), J_m is the rotor inertia, b_c is the viscous friction coefficient, k_t is the motor constant, $i_a(t)$ is the armature current, L_a is the armature inductance, R_a is the armature resistance, k_v is the back electromotive force (EMF) coefficient, V_a is the input DC voltage, and $\tau_{\mathrm{d}}(t)$ is the external unknown disturbance.

Assume that $\omega^*(t)$ is the reference speed. By assigning the state vector $z = [z_1, z_2]^{\mathrm{T}}$, where $z_1 = \omega^*(t) - \omega(t)$ and $z_2 = (b_c/J_m)\omega(t) - (2k_t/J_m)i_a(t) + \dot{\omega}^*(t)$, system (1) can be rewritten as

$$\begin{cases} \dot{z}_1 = z_2 + d_1(t), \\ \dot{z}_2 = a(z,t) + b_o u + d_2(t) \end{cases} \tag{2}$$

where

$$\begin{aligned} a(z,t) &= \ddot{\omega}^*(t) + \left(\frac{2k_t k_v}{J_m L_a} + \frac{R_a b_c}{J_m L_a}\right)[\omega^*(t) - z_1] \\ &\quad + \left(\frac{b_c}{J_m} + \frac{R_a}{L_a}\right)[\dot{\omega}^*(t) - z_2], \\ d_1(t) &= \frac{1}{J_m}\tau_{\mathrm{d}}, \quad d_2(t) = -\frac{b_c}{J_m^2}\tau_{\mathrm{d}}, \quad b_o = -\frac{k_t V_a}{J_m L_a}. \end{aligned}$$

For system (2), it is easy to obtain that the input matrix $B = [0\ b_o]^{\mathrm{T}}$ and output matrix $C = [1\ 0]$, respectively.

In many industrial applications, the BLDC drives are only equipped with three Hall-effect sensors which give three 180° overlapping signals. On this occasion, the angular velocity is derived from the sensor output signals and the armature current is not measurable. Some implementation issues arise when applying the existing SMC approaches to the motion control system (1)

(i) Since the full-state information is required for the controller design, the DOB-based SMC methods proposed in [14, 19] are not applicable if the state z_2 is unavailable.
(ii) It is obvious that the matrix product $CB = 0$ and the mismatched disturbance $d_1(t)$ contains the time-varying load disturbances. As such, the direct output-based control algorithms proposed in [21–24] cannot be directly implemented.

In order to tackle these limitations, we aim at proposing an output feedback-based SMC for a class of n-order dynamic system in the presence of both mismatched and matched disturbances [27], depicted by

$$\begin{cases} \dot{z}_i = z_{i+1} + d_i(t), \quad i = 1, \ldots, n-1, \\ \dot{z}_n = a(z,t) + b_o u + d_n(t), \\ y = z_1 \end{cases} \tag{3}$$

where $z = [z_1, \ldots, z_n]^{\mathrm{T}}$ is the system state vector, $d_i(t)$ and $d_n(t)$ denote the mismatched and matched disturbances, respectively, $a(z,t)$ is the smooth function with respect to z, and b_o is the nominal physical parameter.

3 Main results

Assumption 1: The disturbance $d_i(t), i = 1, \ldots, n-1$ in system (3) is at least $(n-i+r)$th order differentiable, where r is the order of the later designed HOESO.

Remark 1: Assumption 1 is generally a basic premise for SMC design for high-order non-linear systems with mismatched disturbances. A similar one can also be found in the existing results [19, 27]. From the viewpoint of practical applications, $d_i(t)$ is preferably a smooth and continuous signal.
To begin with, by introducing a set of auxiliary variables as

$$\begin{aligned} x_1 &= z_1, \\ x_i &= \frac{1}{l^{i-1}}\left(z_i + \sum_{k=1}^{i-1} d_k^{(i-k-1)}(t)\right), \quad i = 2, \ldots, n, \\ v &= \frac{1}{l^n}u, \end{aligned} \tag{4}$$

system (3) is transformed into

$$\begin{cases} \dot{x}_i = l x_{i+1}, \quad i = 1, \ldots, n-1, \\ \dot{x}_n = \dfrac{1}{l^{n-1}} f(\bar{x}_n, t) + l b_o v + \dfrac{1}{l^{n-1}} d(t) \end{cases} \tag{5}$$

where $\bar{x}_n = [x_1, \ldots, x_n]^{\mathrm{T}}$, l is the scaling gain to be designed later, $f(\bar{x}_n, t)$ is the smooth function with nominal physical parameters in terms of $\bar{x}_n$, and $d(t)$ is the lumped disturbance denoting as

$$d(t) = a(z,t) - f(\bar{x}_n, t) + \sum_{i=1}^{n} d_i^{(n-i)}(t). \tag{6}$$

Remark 2: In practical applications, parameter uncertainties inevitably exist. Given this fact, we introduce $f(\bar{x}_n, t)$ to denote the system known dynamics with nominal physical parameters. Then, $a(z,t) - f(\bar{x}_n, t)$ can be treated as the internal uncertain dynamics and included in the lumped disturbance $d(t)$. Consequently, $d(t)$ represents the combined effects of internal uncertain dynamics and external disturbances.

For simplicity, system (5) can be further rewritten in the compact form as

$$\begin{cases}\dot{\bar{x}}_n = lA_n\bar{x}_n + F_n(\bar{x}_n, t) + lb_oB_nv + \Delta_n(\bar{x}_n, t),\\ y = C_n\bar{x}_n\end{cases} \tag{7}$$

where

$$A_n = \begin{bmatrix}0_{(n-1)\times 1} & I_{(n-1)\times(n-1)}\\ 0_{1\times 1} & 0_{1\times(n-1)}\end{bmatrix},$$
$$B_n = \begin{bmatrix}0_{(n-1)\times 1}\\ 1_{1\times 1}\end{bmatrix},\quad C_n = \begin{bmatrix}1_{1\times 1}\\ 0_{(n-1)\times 1}\end{bmatrix}^{\mathrm{T}},$$
$$F_n(\bar{x}_n, t) = \begin{bmatrix}0_{(n-1)\times 1}\\ \dfrac{f(\bar{x}_n, t)}{l^{n-1}}\end{bmatrix},\quad \Delta_n(\bar{x}_n, t) = \begin{bmatrix}0_{(n-1)\times 1}\\ \dfrac{d(t)}{l^{n-1}}\end{bmatrix}.$$

In order to realise the output feedback controller design for system (7), the unmeasurable auxiliary states $x_i, i = 2, \ldots, n$ as well as the disturbance $d(t)$ should be estimated primarily.

3.1 higher-order ESO

Assumption 2: The smooth function $f(\bar{x}_n, t)$ is global Lipschitz with respect to $\bar{x}_n$, i.e. $\forall t \geq 0, x = [x_1, \ldots, x_n]^{\mathrm{T}}, y = [y_1, \ldots, y_n]^{\mathrm{T}}$,

$$|f(x_1, x_2, \ldots, x_n, t) - f(y_1, y_2, \ldots, y_n, t)| \leq c \parallel x - y \parallel \tag{8}$$

where c is the Lipschitz constant [11, 38].

Assumption 3: The rth-order derivative of $d(t)$ is bounded, i.e. there exists a positive constant $\mathscr{D}$, satisfying $\mathscr{D} = \sup_{t>0} |d^{(r)}(t)|$.

Remark 3: Assumption 3 means that the rate of change of the disturbance is always limited in the physical world, which is a general one made for the higher-order disturbance estimation [36, 39].

With Assumption 3, for any unknown disturbance $d(t)$, it can be represented by the Taylor expansion as follows:

$$d(t) = \sum_{i=0}^{r-1} a_i t^i + \epsilon(t) \tag{9}$$

where $a_i, i = 0, \ldots, r-1$ are the unknown constants and $\epsilon(t)$ is the residual term.

By extending $d^{(i)}(t), i = 0, \ldots, r-1$ as a series of new states, we define

$$x_{n+j} = \frac{1}{l^{n+j-1}} d^{(j-1)}(t),\quad j = 1, \ldots, r. \tag{10}$$

Let $x = [x_1, \ldots, x_{n+r}]^{\mathrm{T}}$. The augmented state-space model is obtained as

$$\begin{cases}\dot{x} = lA_ox + F_o(x, t) + lb_oB_ov + \Delta_o(t),\\ y = C_ox\end{cases} \tag{11}$$

where

$$A_o = \begin{bmatrix}0_{(n+r-1)\times 1} & I_{(n+r-1)\times(n+r-1)}\\ 0_{1\times 1} & 0_{1\times(n+r-1)}\end{bmatrix},$$
$$B_o = \begin{bmatrix}B_n\\ 0_{r\times 1}\end{bmatrix},\quad C_o = \begin{bmatrix}C_n\\ 0_{r\times 1}\end{bmatrix}^{\mathrm{T}},$$
$$F_o(x, t) = \begin{bmatrix}F_n(\bar{x}_n, t)\\ 0_{r\times 1}\end{bmatrix},\quad \Delta_o(t) = \begin{bmatrix}0_{(n+r-1)\times 1}\\ \dfrac{1}{l^{n+r-1}}\epsilon^{(r)}(t)\end{bmatrix}.$$

For system (11), a new HOESO is constructed as

$$\dot{\hat{x}} = lA_o\hat{x} + F_o(\hat{x}, t) + lb_oB_ov + lH(x_1 - \hat{x}_1) \tag{12}$$

where $\hat{x}$ is the estimate of x, $F_o(\hat{x}, t) = [F_n(\hat{\bar{x}}_n, t)^{\mathrm{T}}, 0_{1\times r}]^{\mathrm{T}}$, and $H = [\alpha_1, \ldots, \alpha_{n+r}]^{\mathrm{T}}$ is the observer gain in which $\alpha_i, i = 1, \ldots, n+r$ are selected such that the polynomial

$$\lambda^{n+r} + \alpha_1\lambda^{n+r-1} + \cdots + \alpha_{n+r-1}\lambda + \alpha_{n+r}$$

is Hurwitz.

Lemma 1: Let $V: [0, \infty) \times \mathbb{R}^n \to \mathbb{R}$ be a continuously differentiable function such that

$$\begin{aligned}&\gamma_1(\parallel x \parallel) \leq V(x) \leq \gamma_2(\parallel x \parallel),\\ &\dot{V}(x) \leq -W_3(x),\quad \forall \parallel x \parallel \geq \mu > 0\end{aligned} \tag{13}$$

where γ_1 and γ_2 are class $\mathscr{K}_\infty$ functions and $W_3(x)$ is a continuous positive definite function. Then, for all initial condition $x(t_0)$, there is $T \geq 0$ (dependent on $x(t_0)$ and μ) such that

$$\parallel x(t) \parallel \leq \zeta(\parallel x(t_0) \parallel, t - t_0),\quad \forall t_0 < t < t_0 + T \tag{14}$$

where ζ is a class $\mathscr{KL}$ function and

$$\parallel x(t) \parallel \leq \gamma_1^{-1}(\gamma_2(\mu)),\quad \forall t \geq t_0 + T. \tag{15}$$

The proof of Lemma 1 can be referred to [40, Theorem 4.18].

Theorem 1: Under Assumptions 1–3, with the proper selection of the scaling gain l, the estimation error of the observer (12) is ultimately bounded.

Proof: Define the estimation error $\tilde{x} = x - \hat{x}$. Combining (11) with (12), the error dynamics are governed by

$$\dot{\tilde{x}} = l\bar{A}_o\tilde{x} + \tilde{F}_o + \Delta_o(t) \tag{16}$$

where $\bar{A}_o = A_o - HC_o$, $\tilde{F}_o = F_o(x, t) - F_o(\hat{x}, t)$.

Since $\bar{A}_o$ is Hurwitz, there exists a positive definite matrix P_o satisfying the Lyapunov equation $\bar{A}_o^{\mathrm{T}}P_o + P_o\bar{A}_o = -I_{(n+r)\times(n+r)}$. Consider the following quadratic Lyapunov function as $V_1(\tilde{x}) = \tilde{x}^{\mathrm{T}}P_o\tilde{x}$. The following inequalities can be easily verified:

$$\lambda_{\min}(P_o) \parallel \tilde{x} \parallel^2 \leq V_1(\tilde{x}) \leq \lambda_{\max}(P_o) \parallel \tilde{x} \parallel^2, \tag{17}$$

$$\parallel \frac{\partial V_1(\tilde{x})}{\partial \tilde{x}} \parallel = \parallel 2\tilde{x}^{\mathrm{T}}P_o \parallel \leq 2 \parallel P_o \parallel \parallel \tilde{x} \parallel = 2\lambda_{\max}(P_o) \parallel \tilde{x} \parallel \tag{18}$$

where $\lambda_{\min}\{\bullet\}$ and $\lambda_{\max}\{\bullet\}$ denote the minimum and maximum eigenvalues of a symmetric matrix, respectively.

Taking the derivative of $V_1(\tilde{x})$ yields

$$\dot{V}_1(\tilde{x}) = -l\tilde{x}^{\mathrm{T}}\tilde{x} + 2\tilde{F}_o^{\mathrm{T}}P_o\tilde{x} + 2\Delta_o^{\mathrm{T}}(t)P_o\tilde{x}. \tag{19}$$

According to Assumptions 2 and 3, one can obtain that

$$\| \tilde{F}_o \| = \frac{1}{l^{n-1}} | f(\bar{x}_n, t) - f(\hat{\bar{x}}_n, t) | \leq \frac{c}{l^{n-1}} \| \tilde{x} \| \tag{20}$$

and

$$\| \Delta_o(t) \| = \left| \frac{1}{l^{n+r-1}} \epsilon^{(r)}(t) \right| = \left| \frac{1}{l^{n+r-1}} d^{(r)}(t) \right| \leq \frac{\mathscr{D}}{l^{n+r-1}}. \tag{21}$$

Substituting (18), (20), and (21) into (19) yields

$$\begin{aligned} \dot{V}_1(\tilde{x}) &\leq -\left(l - \frac{2\lambda_{\max}(P_o)c}{l^{n-1}} \right) \| \tilde{x} \|^2 + \frac{2\lambda_{\max}(P_o)\mathscr{D}}{l^{n+r-1}} \| \tilde{x} \| \\ &= -(1-\theta)\left(l - \frac{2\lambda_{\max}(P_o)c}{l^{n-1}} \right) \| \tilde{x} \|^2 - M(\tilde{x}) \end{aligned} \tag{22}$$

where $0 < \theta < 1$ and

$$M(\tilde{x}) = \underbrace{\left[\left(l - \frac{2\lambda_{\max}(P_o)c}{l^{n-1}} \right) \theta \| \tilde{x} \| - \frac{2\lambda_{\max}(P_o)\mathscr{D}}{l^{n+r-1}} \right]}_{N(\tilde{x})} \| \tilde{x} \|.$$

Thus,

$$\forall \| \tilde{x} \| \geq \frac{2\lambda_{\max}(P_o)\mathscr{D}}{\theta l^r [l^n - 2\lambda_{\max}(P_o)c]} := \mu > 0, \tag{23}$$

we have $M(\tilde{x}) = N(\tilde{x}) \| \tilde{x} \| \geq 0$. In this regard, inequality (22) satisfies

$$\begin{aligned} \dot{V}_1(\tilde{x}) &\leq -(1-\theta)\left(l - \frac{2\lambda_{\max}(P_o)c}{l^{n-1}} \right) \| \tilde{x} \|^2 \\ &:= -W_3(x), \quad \forall \| \tilde{x} \| \geq \mu > 0. \end{aligned} \tag{24}$$

To guarantee the stability of the observer, the scaling gain l should be selected to satisfy the condition

$$l > \sqrt[n]{2\lambda_{\max}(P_o)c}. \tag{25}$$

Let $\gamma_1(\| \tilde{x} \|) := \lambda_{\min}(P_o) \| \tilde{x} \|^2, \gamma_2(\| \tilde{x} \|) := \lambda_{\max}(P_o) \| \tilde{x} \|^2$. By using (17) and (24), it follows from Lemma 1 that the estimation error is globally uniformly bounded by

$$\mathscr{B}_o = \left\{ \tilde{x} \middle| \| \tilde{x} \| \leq \gamma_1^{-1}(\gamma_2(\mu)) = \mu \sqrt{\frac{\lambda_{\max}(P_o)}{\lambda_{\min}(P_o)}} \right\}. \tag{26}$$

This completes the proof. □

Remark 4: It can be inferred from (23) and (26) that the estimation error can be arbitrarily reduced by increasing l. However, it is worth noting that too large l may lead to undesirable dynamic performances such as the peaking phenomenon and the noise amplification, especially when the initial estimation error is large. To attenuate the negative impacts caused by the high-gain action, a relatively larger order r is expected to be selected such that the higher observation accuracy can be obtained. For instance, one can achieve global asymptotic stability for the observer by choosing $r = 1, 2$, and 3 while tackling the disturbances with the types of constant, ramp, and parabolic, respectively. In this case, l only needs to be selected to satisfy the condition (25). While tackling the more general order disturbances, e.g. the polynomial disturbance, the higher order r is selected, the smaller residual term is remained, which assures that the tinier convergence domain can be reached. However, this induces the increase of computational burden unavoidably. To this end, the compromise should be made to balance among the steady-state accuracy, dynamic performance and computational burden by choosing appropriate l and r for different control systems.

Remark 5: The newly designed HOESO is different from that proposed in [35, 37]. The difference lies in whether the known dynamics $f(\bar{x}_n, t)$ is treated as an uncertainty and lumped into the disturbance $d(t)$. In the standard ESO framework, in order to counteract the negative impacts caused by $f(\bar{x}_n, t)$ in addition to $d(t)$, a larger scaling gain l is generally required. In our design, $f(\bar{x}_n, t)$ and $d(t)$ are handled separately since the nominal physical parameters are usually known as a priori and $\bar{x}_n$ is synchronously estimated, which guarantees the higher observation accuracy while selecting the same scaling gain l in comparison with [35, 37].

3.2 Output feedback-based SMC

Depending on the estimated states $\hat{x}_i, i = 1, \ldots, n$, the sliding surface is designed as

$$s = K\hat{x} = \sum_{i=1}^{n} \beta_i \hat{x}_i \tag{27}$$

where $K = [K_c, \beta_n, 0_{1\times r}]$, in which $K_c = [\beta_1, \ldots, \beta_{n-1}]$ and β_i, $i = 1, \ldots, n-1$ are selected such that the polynomial $\lambda^{n-1} + \beta_{n-1}\lambda^{n-2} + \cdots + \beta_2\lambda + \beta_1$ is Hurwitz, $\beta_n = 1$.

The proposed output feedback-based SMC is given by

$$u = -\frac{l^n}{b_o}\left(\sum_{i=1}^{n} \beta_i \hat{x}_{i+1} + \frac{1}{l^n} f(\hat{x}, t) + k_1 \text{sign}(s) + k_2 s \right) \tag{28}$$

where l, k_1, and k_2 are the parameters to be designed.

Theorem 2: Under Assumptions 1–3, the control law (28) could drive the system output y to an ultimately bounded region if the control gains k_1 and k_2 are designed to satisfy the condition

$$k_1 = \rho + |\tilde{x}_1| \sum_{i=1}^{n} \alpha_i \beta_i, k_2 > 0 \tag{29}$$

where ρ is a sufficiently small positive constant; the scaling gain l is selected to satisfy the condition

$$l > \max \{ \sqrt[n]{2\lambda_{\max}(P_o)c}, \sqrt[n]{2\lambda_{\max}(P_c)c} \} \tag{30}$$

where P_c is a positive definite matrix given in (39).

Proof: The proof is divided into two steps. The first step is to prove that the system states can reach the sliding surface in finite time and the second step is to demonstrate that the output is ultimately bounded after the sliding surface is reached.

Step 1: Taking the derivative of s, we have

$$\begin{aligned} \dot{s} &= \sum_{i=1}^{n-1} \beta_i \dot{\hat{x}}_i + \dot{\hat{x}}_n \\ &= l \sum_{i=1}^{n-1} \beta_i \hat{x}_{i+1} + l\tilde{x}_1 \sum_{i=1}^{n-1} \alpha_i \beta_i + \dot{\hat{x}}_n \\ &= l \sum_{i=1}^{n} \beta_i \hat{x}_{i+1} + l\tilde{x}_1 \sum_{i=1}^{n} \alpha_i \beta_i + \frac{f(\hat{x}, t)}{l^{n-1}} + l b_o v. \end{aligned} \tag{31}$$

Substituting the control law (28) into (31) yields

$$\dot{s} = -l\left(k_1 \text{sign}(s) + k_2 s - \tilde{x}_1 \sum_{i=1}^{n} \alpha_i \beta_i \right). \tag{32}$$

Consider a Lyapunov function candidate as $V_2(s) = 1/2s^2$. Taking the derivative of $V_2(s)$ with the substitution of (32), yields

$$\begin{aligned}\dot{V}_2(s) &= -lk_1|s| - lk_2 s^2 + l\tilde{x}_1 s\sum_{i=1}^{n}\alpha_i\beta_i \\ &\le -l\left(k_1 - |\tilde{x}_1|\sum_{i=1}^{n}\alpha_i\beta_i\right)|s| - lk_2 s^2 .\end{aligned} \tag{33}$$

With the condition (29) in mind, (33) can be further transformed into

$$\dot{V}_2(s) \le -\sqrt{2}l\rho V_2^{1/2} - 2lk_2 V_2 . \tag{34}$$

It can be inferred from Remark 2 in [41] that the system states will reach the defined sliding surface (27) in finite time T_r, where

$$T_r \le \frac{1}{lk_2}\ln\left(1 + \frac{\sqrt{2}k_2}{\rho}V_2^{1/2}(s(0))\right). \tag{35}$$

Note that the condition (25) should be always satisfied in order to guarantee the boundness of the estimation error.

Step 2: Once the sliding surface is reached, we have

$$0 = \sum_{i=1}^{n-1}\beta_i\hat{x}_i + \hat{x}_n = \frac{\dot{x}_{n-1}}{l} + \sum_{i=1}^{n-1}\beta_i x_i - \sum_{i=1}^{n}\beta_i\tilde{x}_i . \tag{36}$$

Define $\bar{x}_{n-1} = [x_1, \ldots, x_{n-1}]^{\mathrm{T}}$. System (36) can be rewritten in the compact form as

$$\dot{\bar{x}}_{n-1} = l\bar{A}_c\bar{x}_{n-1} + B_{n-1}K\tilde{x} \tag{37}$$

where

$$\bar{A}_c = A_{n-1} - B_{n-1}K_c,$$
$$A_{n-1} = \begin{bmatrix} 0_{(n-2)\times 1} & I_{(n-2)\times(n-2)} \\ 0_{1\times 1} & 0_{1\times(n-2)} \end{bmatrix}, \quad B_{n-1} = \begin{bmatrix} 0_{(n-2)\times 1} \\ 1_{1\times 1} \end{bmatrix}.$$

Combining (16) and (37) together, the closed-loop system is governed by

$$\dot{\eta} = lA\eta + \Phi(\eta, t) \tag{38}$$

where

$$\eta = \begin{bmatrix} \bar{x}_{n-1} \\ \tilde{x} \end{bmatrix}, \quad A = \begin{bmatrix} \bar{A}_c & B_{n-1}K \\ 0 & \bar{A}_o \end{bmatrix}, \quad \Phi = \begin{bmatrix} 0 \\ \tilde{F}_o + \Delta_o(x,t) \end{bmatrix}.$$

Since both $\bar{A}_c$ and $\bar{A}_o$ are the Hurwitz matrices, it is easy to verify that A is also a Hurwitz matrix. Therefore, there exists a positive definite matrix P_c satisfying the Lyapunov equation

$$A^{\mathrm{T}}P_c + P_c A = -I_{(2n+r-1)\times(2n+r-1)} . \tag{39}$$

Next, considering the Lyapunov function candidate for system (38) as $V_3(\eta) = \eta^{\mathrm{T}}P_c\eta$, where $\eta = [\bar{x}_{n-1}^{\mathrm{T}}, \tilde{x}^{\mathrm{T}}]^{\mathrm{T}}$. Taking the derivative of $V_3(\eta)$ yields

$$\dot{V}_3(\eta) = -l\eta^{\mathrm{T}}\eta + 2\Phi(\eta, t)P_c\eta . \tag{40}$$

Note that

$$\| \Phi(\eta, t) \| \le \| \tilde{F}_o \| + \| \Delta_o(x,t) \| \le \frac{c}{l^{n-1}}\| \eta \| + \frac{\mathscr{D}}{l^{n+r-1}} . \tag{41}$$

Substituting (41) into (40) yields

$$\dot{V}_3 \le -l\| \eta \|^2 + \frac{2\lambda_{\max}(P_c)c}{l^{n-1}}\| \eta \|^2 + \frac{2\lambda_{\max}(P_c)\mathscr{D}}{l^{n+r-1}}\| \eta \| . \tag{42}$$

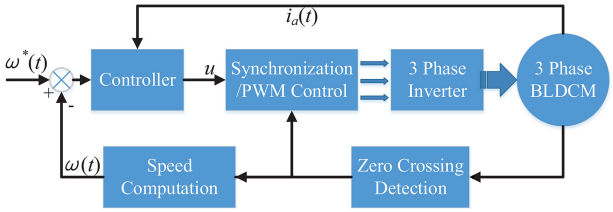

Fig. 1 *Structure of BLDCM drive system*

The following steps are similar with (22)–(24), which are omitted here for simplicity. Likewise, to guarantee the stability of the closed-loop system (38), l should be selected to satisfy

$$l > \sqrt[n]{2\lambda_{\max}(P_c)c} . \tag{43}$$

Combining (43) with (25), the condition (30) is thus attained.

Moreover, it can be concluded that the system states are ultimately bounded by the region

$$\mathscr{B}_o = \left\{\eta \middle| \| \eta \| \le \frac{2\lambda_{\max}(P_c)\mathscr{D}}{\theta l^r[l^n - 2\lambda_{\max}(P_c)c]}\sqrt{\frac{\lambda_{\max}(P_c)}{\lambda_{\min}(P_c)}}\right\}. \tag{44}$$

This completes the proof. □

Remark 6: Particularly, if the high-frequency terms in $d(t)$ are small enough to be negligible, that is $\epsilon(t) = 0$, then (42) can be rewritten as

$$\dot{V}_3 \le -\left(l - \frac{2\lambda_{\max}(P_c)c}{l^{n-1}}\right)\| \eta \|^2 . \tag{45}$$

Therefore, the globally asymptotic stability can be achieved.

Remark 7: As compared to the results presented in [25, 26], the upper bound of the time-varying disturbances is not necessary to be known as a priori in the proposed control law (28). Condition (29) reveals that the switching gain k_1 is adaptively chosen based on the estimation error $\tilde{x}_1$. Since the steady-state value of $\tilde{x}_1$ can be regulated arbitrarily small by selecting proper l and r, the chattering problem will be alleviated remarkably.

4 Application to a BLDCM drive system

The output feedback-based SMC design for the speed regulation of a BLDCM which is subject to the mismatched disturbances is investigated in this section.

The BLDCM is an AC synchronous motor with permanent magnets on the rotor and windings on the stator. Such motors combine high efficiency with high reliability, and for a lower cost in comparison with brush motors. Usually, the dynamic model of a BLDCM can be expressed as (1). It can be easily observed that the speed regulation performance is mainly affected by the external uncertain disturbances. To this end, the control objective is to design an advanced controller to realise the fast and high-precision speed tracking. The typical structure of the BLDCM drive system is shown in Fig. 1.

4.1 Controller design

It is assumed that only the state variable $\omega(t)$ is available. Introducing an auxiliary state vector $x = [x_1, x_2]^{\mathrm{T}}$, where

$$\begin{aligned} x_1 &= \omega^*(t) - \omega(t), \\ x_2 &= \frac{1}{l}\left(\frac{b_c}{J_m}\omega(t) - \frac{2k_t}{J_m}i_a(t) + \frac{\tau_{\mathrm{d}}(t)}{J_m} + \dot{\omega}^*(t)\right). \end{aligned} \tag{46}$$

In view of (46), system (1) can be rewritten as

$$\begin{cases} \dot{x}_1 = l x_2, \\ \dot{x}_2 = \dfrac{1}{l} f(x,t) + \dfrac{b_o}{l} u + \dfrac{d(t)}{l} \end{cases} \tag{47}$$

where

$$f(x,t) = \ddot{\omega}^*(t) + \left(\frac{2k_t k_v}{J_m L_a} + \frac{R_a b_c}{J_m L_a}\right)[\omega^*(t) - x_1] + \left(\frac{b_c}{J_m} + \frac{R_a}{L_a}\right)[\dot{\omega}^*(t) - l x_2],$$

$$d(t) = \frac{R_a}{J_m L_a}\tau_{\mathrm{d}} + \frac{1}{J_m}\dot{\tau}_{\mathrm{d}}, \quad b_o = -\frac{k_t V_a}{J_m L_a}.$$

It is obvious that $f(x,t)$ satisfies the Lipschitz condition with respect to x, where the Lipschitz constant c equals to $(2k_t k_v + R_a b_c + l b_c L_a + l R_a L_a)/(J_m L_a)$.

On the basis of the HOESO presented above, by selecting $r = 3$, the observer is constructed as

$$\begin{cases} \dot{\hat{x}}_1 = l\hat{x}_2 + \alpha_1 l(x_1 - \hat{x}_1),\ \hat{x}_1(0) = \omega^*(0), \\ \dot{\hat{x}}_2 = l\hat{x}_3 + \dfrac{1}{l} f(\hat{x},t) + \dfrac{b_o}{l} u + \alpha_2 l(x_1 - \hat{x}_1),\ \hat{x}_2(0) = 0, \\ \dot{\hat{x}}_3 = l\hat{x}_4 + \alpha_3 l(x_1 - \hat{x}_1),\ \hat{x}_3(0) = 0, \\ \dot{\hat{x}}_4 = l\hat{x}_5 + \alpha_4 l(x_1 - \hat{x}_1),\ \hat{x}_4(0) = 0, \\ \dot{\hat{x}}_5 = \alpha_5 l(x_1 - \hat{x}_1),\ \hat{x}_5(0) = 0, \end{cases} \tag{48}$$

where $\hat{x}_i, i = 1, \ldots, 5$ are the estimates of x_1, x_2, $(1/l^2)d$, $(1/l^3)\dot{d}$, and $(1/l^4)d^{(2)}$, respectively and α_i, $i = 1, \ldots, 5$ are selected such that the polynomial $\lambda^5 + \alpha_1\lambda^4 + \cdots + \alpha_4\lambda + \alpha_5$ is Hurwitz.

The sliding surface is designed as

$$s = \beta_1 \hat{x}_1 + \hat{x}_2 \tag{49}$$

where $\beta_1 > 0$. The control law for the BLDCM drive system is designed as

$$u = -\frac{l^2}{b_o}\left(\beta_1 \hat{x}_2 + \hat{x}_3 + \frac{1}{l^2} f(\hat{x},t) + k_1 \mathrm{sign}(s) + k_2 s\right). \tag{50}$$

According to Theorem 2, the designed parameters should satisfy the following conditions:

$$\begin{aligned} & l > \sqrt{2c}\ \max\{\sqrt{\lambda_{\max}(P_o)}, \sqrt{\lambda_{\max}(P_c)}\}, \\ & k_1 = \rho + (\alpha_1\beta_1 + \alpha_2)|\tilde{x}_1|, \quad k_2 > 0 \end{aligned} \tag{51}$$

where P_o and P_c are the positive definite matrices satisfying the function $\bar{A}_o^{\mathrm{T}} P_o + P_o \bar{A}_o = -I_5$ and $A^{\mathrm{T}} P_c + P_c A = -I_6$, with

$$\bar{A}_o = \begin{bmatrix} -\alpha_1 & 1 & 0 & 0 & 0 \\ -\alpha_2 & 0 & 1 & 0 & 0 \\ -\alpha_3 & 0 & 0 & 1 & 0 \\ -\alpha_4 & 0 & 0 & 0 & 1 \\ -\alpha_5 & 0 & 0 & 0 & 0 \end{bmatrix}, \quad A = \begin{bmatrix} -\beta_1 & \beta_1 & 1 & 0 & 0 & 0 \\ 0 & -\alpha_1 & 1 & 0 & 0 & 0 \\ 0 & -\alpha_2 & 0 & 1 & 0 & 0 \\ 0 & -\alpha_3 & 0 & 0 & 1 & 0 \\ 0 & -\alpha_4 & 0 & 0 & 0 & 1 \\ 0 & -\alpha_5 & 0 & 0 & 0 & 0 \end{bmatrix}.$$

4.2 Experimental results

To investigate the efficiency of the proposed method, the experimental bench of the BLDCM is set up as shown in Fig. 2. The platform TMDSHVMTRPFCKIT explored by Texas Instrument provides the integrated control and drive circuits, e.g. TMS320F28335 control card, three-phase inverter stage, AC rectifier, over-current protection and so on. Three Hall-effect sensors are wired to the input capture pins of the control card and the speed information is available by measuring the time interval between two input captures. The magnetic powder brake is utilised to generate the time-varying disturbance, which is controlled by a tension controller through an external input analogue interface. An isolated transformer is also adopted to enhance the system security for the experimental tests. In addition, a host computer is used to realise the C-program development and data acquisition via USB and UART communication, respectively. Fig. 3 shows the implementation architecture. The parameters of the adopted BLDCM are listed in Table 1.

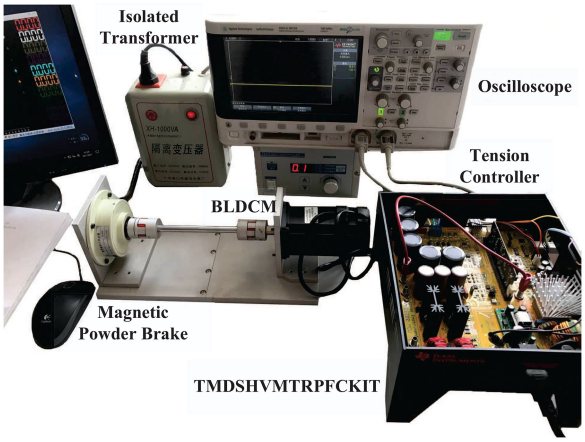

Fig. 2 *Experimental setup*

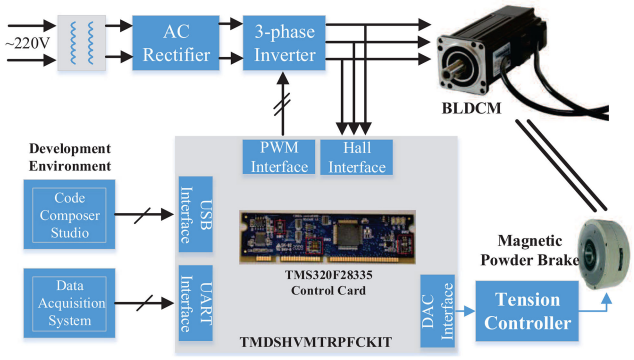

Fig. 3 *Implementation architecture*

Table 1 Parameters of BLDCM

Parameters	Meaning	Value
n_p	pole numbers	8
V_a	rated voltage	310 V
N	rated speed	3500 r/min
R_a	armature resistance	17 Ω
L_a	armature inductance	7 mH
k_t	torque coefficient	0.362 N · m/A
k_v	back-EMF coefficient	0.425 V/(rad/s)
b_c	viscous friction coefficient	7×10^{-5} N · m · s/rad
J_m	moment of inertial	1.25×10^{-3} kg · m^2

In order to implement the algorithms (48)–(50) in a digital chip, the continuous control laws should be discretised first. Suppose that the sampling period of the control system is h ($h = 50\,\mu$s in this paper). The discrete version of a continuous signal $x(t)$ can be $x(kh)$, where $k \in \mathbb{N}+$. For a differential signal $\dot{x}(t)$, by using Euler discretisation, the general discrete version is $[x((k+1)h) - x(kh)]/h$.

4.2.1 Control performance: To investigate the control performance of the proposed method, two experimental tests are carried out as follows:

Case I: $\omega^*(t) = 1000$ r/min and $\tau_{\mathrm{d}} = 0.4$ N · m when $t > 5$ s.

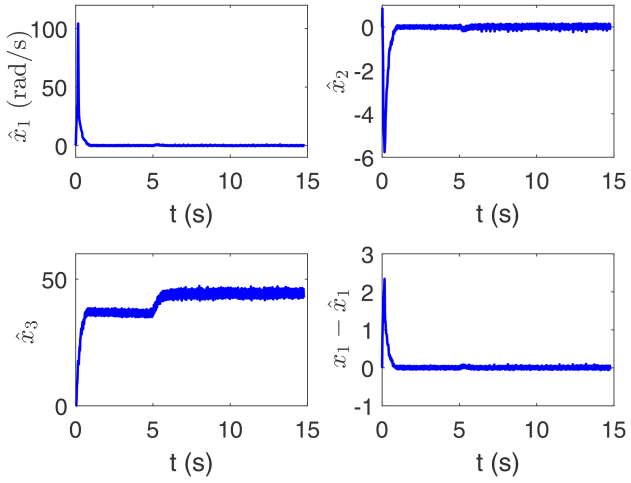

Fig. 4 *Observation performance of HOESO in Case I*

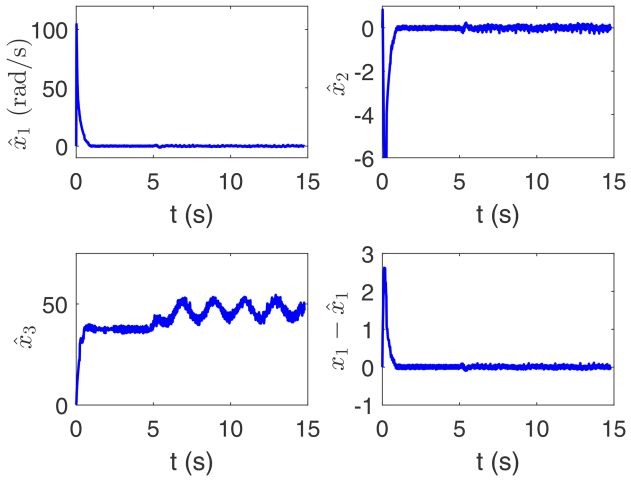

Fig. 5 *Observation performance of HOESO in Case II*

Case II: $\omega^*(t) = 1000\,\mathrm{r/min}$ and $\tau_\mathrm{d} = 0.2\sin(\pi t) + 0.4\,\mathrm{N}\cdot\mathrm{m}$ when $t > 5\,\mathrm{s}$.

The observer gains in the experimental test are selected as $\alpha_1 = \alpha_2 = 2.5, \alpha_3 = 1.25,\ \alpha_4 = 0.31, \alpha_5 = 0.03$. Using Matlab to solve the Lyapunov equations, we can obtain that the eigenvalues of P_o and P_c satisfy $\lambda_{\max}(P_o) \simeq 16,\ \lambda_{\max}(P_c) \simeq 20$, respectively. According to the parameter selection criteria (51), we choose $l = 375, \beta_1 = 4.5, \theta = 0.3, \rho = 0.05$, and $k_2 = 1.25$.

The observation results of the proposed HOESO are shown in Figs. 4 and 5. It shows that both the states and the time-varying disturbance are effectively estimated. Figs. 6*a* and 7*a* present the speed tracking results. In general, the proposed control approach obtains the satisfactory performance in terms of both the transient and steady-state natures. When $t < 5\,\mathrm{s}$, i.e. in the absence of the external disturbance, the speed tracks the reference signal rapidly and offset-free. After the disturbance is imposed, the steady-state offsets of the output caused by the mismatched disturbance τ_d are entirely removed. Moreover, as shown in Figs. 6*b* and 7*b*, the control chattering is significantly reduced with the aid of HOESO. This is owing to that the switching gain k_1 is adaptively chosen based on the estimation error $\tilde{x}_1$. The real-time values of k_1 under two different cases are depicted in Figs. 6c and 7c.

Fig. 8 shows the speed response curves under the different scaling gains. It is observed from Fig. 8*b* that the disturbance rejection ability is enhanced by tuning up l. However, too large l may lead to the excessive transient overshoot (see Fig. 8*a*) and noise amplification. As stated in Remark 4, the compromise should be made to balance between the disturbance rejection performance and steady-state accuracy by choosing proper l in the engineering.

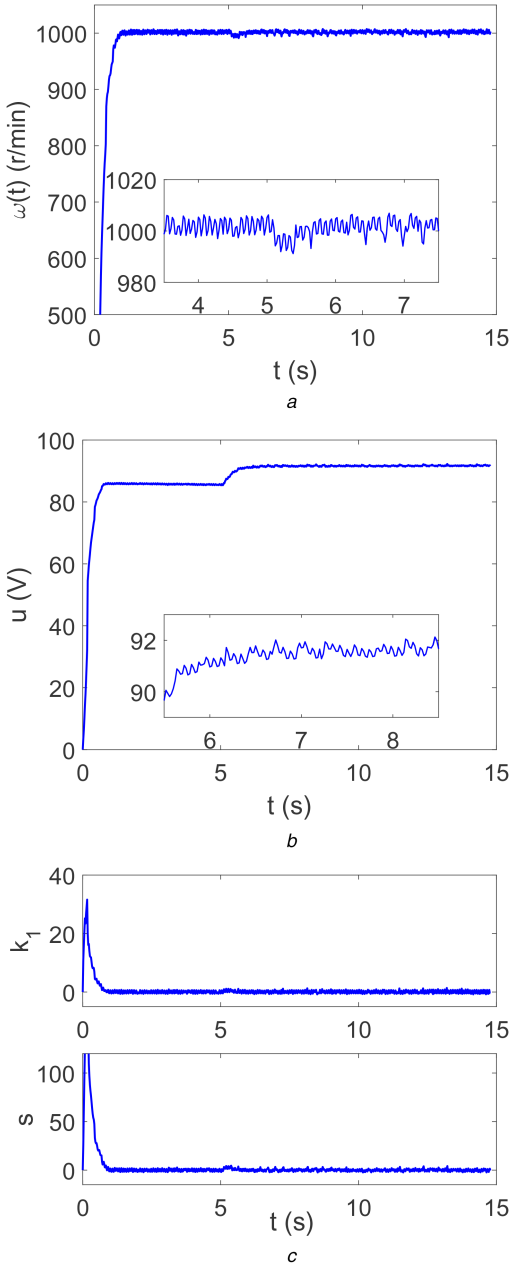

Fig. 6 *Response curves under the proposed method in Case I*
(a) Speed, ***(b)*** Control input, ***(c)*** Sliding variable and switching gain

4.2.2 Comparative results: To further evaluate the effectiveness of the proposed HOESO-SMC method, the PI control and the ESO-based SMC (ESO-SMC) schemes are introduced for the performance comparison.

The comparative experiments are conducted under Case II with sinusoidal disturbances. The employed two control schemes are designed as follows:

(1) PI control

$$u = -\frac{l^2}{b_o}\left(k_\mathrm{p}x_1 + k_\mathrm{i}\int_0^t x_1\,\mathrm{d}\tau\right). \tag{52}$$

(2) ESO-SMC

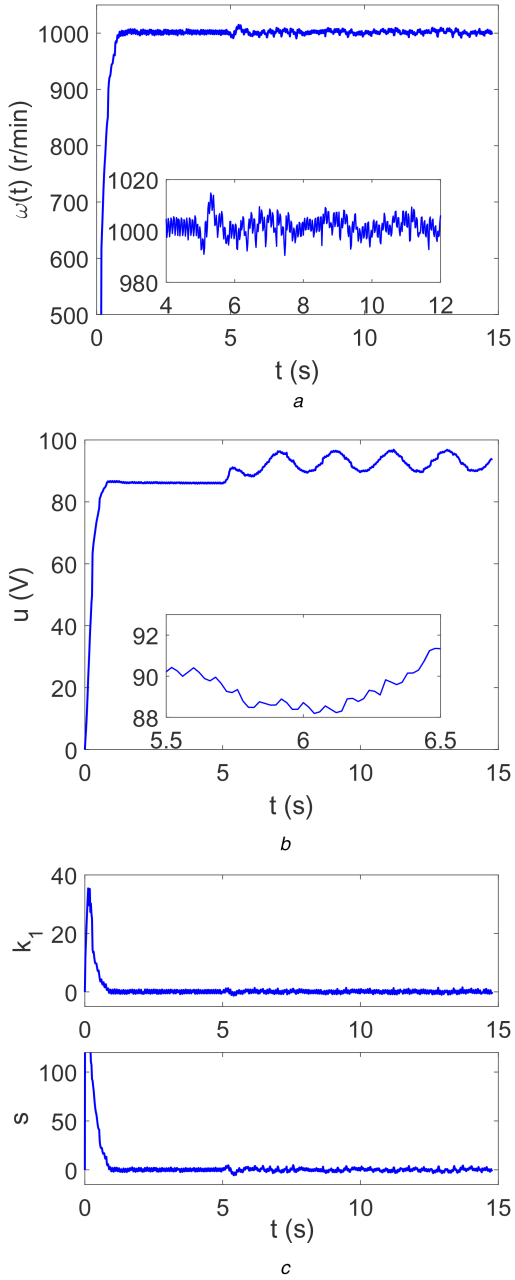

Fig. 7 *Response curves under the proposed method in Case II*
(a) Speed, ***(b)*** Control input, ***(c)*** Sliding variable and switching gain

$$\begin{cases} \dot{\hat{x}}_1 = l\hat{x}_2 + 2.5l(x_1 - \hat{x}_1), \quad \hat{x}_1(0) = \omega^*(0), \\ \dot{\hat{x}}_2 = l\hat{x}_3 + \dfrac{b_o}{l}u + 2.5l(x_1 - \hat{x}_1), \quad \hat{x}_2(0) = 0, \\ \dot{\hat{x}}_3 = 1.25l(x_1 - \hat{x}_1), \quad \hat{x}_3(0) = 0, \\ s = \beta_1\hat{x}_1 + \hat{x}_2, \\ u = -\dfrac{l^2}{b_o}[\beta_1\hat{x}_2 + \hat{x}_3 + k_1\text{sign}(s) + k_2 s]. \end{cases} \tag{53}$$

To have a fair comparison, the control gains of ESO-SMC are selected equally with the proposed method. For PI control, the parameters are selected as $k_p = k_2\beta_1$ and $k_i = 0.1k_p$.

As shown in Fig. 9*a*, it is obviously seen that the proposed method achieves the fastest convergence rate in comparison with the PI control and ESO-SMC schemes. When the sinusoidal disturbance is applied to the motor, the proposed method holds the superior robustness against the mismatched disturbance, while it only guarantees the speed tracking errors converge to a relatively larger region by means of the other two methods under the same test conditions.

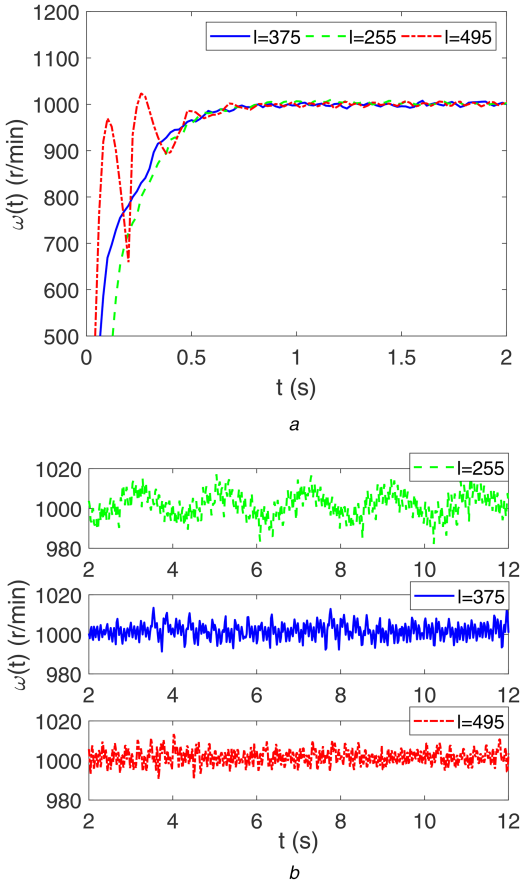

Fig. 8 *Speed responses with different scaling gains*
(a) Transient responses, ***(b)*** Steady-state responses

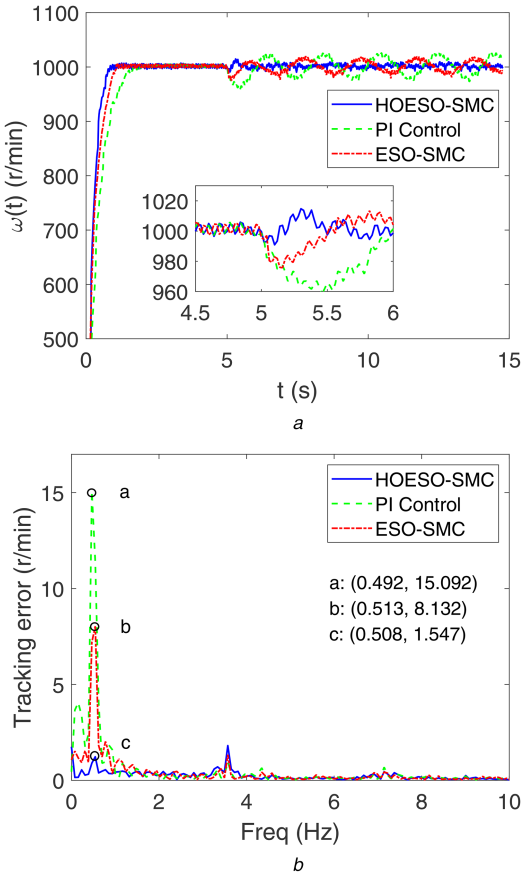

Fig. 9 *Performance comparison among different controllers*
(a) Speed responses, ***(b)*** Amplitude spectrum of the speed tracking errors

To observe the disturbance rejection performance under different controllers, the fast Fourier transformation technique is introduced. The amplitude spectrum of the speed tracking errors is shown in Fig. 9*b*, where the response curves are converted from the time domain to the frequency domain. It can be seen that the external sinusoidal disturbance with the frequency of 0.5Hz is almost eliminated by the proposed method, which shows the effectiveness of the proposed control scheme on the higher-order disturbance rejection.

5 Conclusion

We have presented an output feedback-based SMC approach for disturbed motion control systems in this paper. A new HOESO has been developed by means of input and output signals to estimate the unmeasurable states as well as the lumped disturbances synchronously. System output has been rendered ultimately bounded even in the presence of mismatched higher-order disturbances. Different from most of the existing output feedback based SMC schemes, the switching gain in the proposed control approach can be adaptively chosen depending on the estimation error generated by HOESO. With this feature, chattering reduction effect is thus attained without sacrificing the disturbance rejection performance. Experimental results on a BLDCM drive system have verified the remarkable merits of the proposed method.

6 Acknowledgments

This work was supported in part by the International Science & Technology Cooperation Program of China (grant no. 2015DFA10490), in part by the National Nature Science Foundation of China (grant nos. 61473080 and 61573099), in part by the Fundamental Research Funds for the Central Universities (grant nos. 2242016R30011 and 2242016K41067) and in part by the Postgraduate Research & Practice Innovation Program of Jiangsu Province (KYLX15_0213).

7 References

[1] Xie, X.J., Tian, J.: 'Adaptive state-feedback stabilization of high-order stochastic systems with nonlinear parameterization', *Automatica*, 2009, **45**, (1), pp. 126–133

[2] Chen, W.H., Ballance, D.J., Gawthrop, P.J.: 'Optimal control of nonlinear systems: a predictive control approach', *Automatica*, 2003, **39**, (4), pp. 633–641

[3] Liu, L., Yang, X.: 'Robust adaptive state constraint control for uncertain switched high-order nonlinear systems', *IEEE Trans. Ind. Electron.*, 2017, **64**, (10), pp. 8108–8117

[4] Levant, A.: 'Higher-order sliding modes, differentiation and outputfeedback control', *Int. J. Control*, 2003, **76**, (9/10), pp. 924–941

[5] Wang, X., Li, S., Yu, X.*, et al.*: 'Distributed active anti-disturbance consensus for leader-follower higher-order multi-agent systems with mismatched disturbances', *IEEE Trans. Autom. Control*, 2017, **62**, (11), pp. 5795–5801

[6] Shtessel, Y., Edwards, C., Fridman, L.*, et al.*: '*Sliding mode control and observation*' (Birkhäuser, New York, 2014)

[7] Ding, S., Zheng, W., Sun, J.*, et al.*: 'Second-order sliding mode controller design and its implementation for buck converters', *IEEE Trans. Ind. Inf.*, 2018, **14**, (5), pp. 1990–2000

[8] Hu, Q., Shao, X., Chen, W.H.: 'Robust fault-tolerant tracking control for spacecraft proximity operations using time-varying sliding mode', *IEEE Trans. Aerosp. Electron. Syst.*, 2018, **54**, (1), pp. 2–17

[9] Darba, A., Belie, F.D., D'haese, P.*, et al.*: 'Improved dynamic behavior in BLDC drives using model predictive speed and current control', *IEEE Trans. Ind. Electron.*, 2016, **63**, (2), pp. 728–740

[10] Yao, J., Jiao, Z., Ma, D.: 'Extended-state-observer-based output feedback nonlinear robust control of hydraulic systems with backstepping', *IEEE Trans. Ind. Electron.*, 2014, **61**, (11), pp. 6285–6293

[11] Guo, Q., Zhang, Y., Celler, B.G.*, et al.*: 'Backstepping control of electro-hydraulic system based on extended-state-observer with plant dynamics largely unknown', *IEEE Trans. Ind. Electron.*, 2016, **63**, (11), pp. 6909–6920

[12] Yang, J., Chen, W.H., Li, S.*, et al.*: 'Disturbance/uncertainty estimation and attenuation techniques in PMSM drive – a survey', *IEEE Trans. Ind. Electron.*, 2017, **64**, (4), pp. 3273–3285

[13] Li, S., Yang, J., Chen, W.H.*, et al.*: 'Generalized extended state observer based control for systems with mismatched uncertainties', *IEEE Trans. Ind. Electron.*, 2012, **59**, (12), pp. 4792–4802

[14] Yang, J., Li, S., Yu, X.: 'Sliding-mode control for systems with mismatched uncertainties via a disturbance observer', *IEEE Trans. Ind. Electron.*, 2013, **60**, (1), pp. 160–169

[15] Cao, W., Xu, J.: 'Nonlinear integral-type sliding surface for both matched and unmatched uncertain systems', *IEEE Trans. Autom. Control*, 2004, **49**, (8), pp. 1355–1360

[16] Rubagotti, M., Estrada, A., Castaños, F.*, et al.*: 'Integral sliding mode control for nonlinear systems with matched and unmatched perturbations', *IEEE Trans. Autom. Control*, 2011, **56**, (11), pp. 2699–2704

[17] Choi, H.H.: 'LMI-based sliding surface design for integral sliding mode control of mismatched uncertain systems', *IEEE Trans. Autom. Control*, 2007, **52**, (4), pp. 736–742

[18] Polyakov, A., Poznyak, A.: 'Invariant ellipsoid method for minimization of unmatched disturbance effects in sliding mode control', *Automatica*, 2011, **47**, (7), pp. 1450–1454

[19] Yang, J., Li, S., Su, J.*, et al.*: 'Continuous nonsingular terminal sliding mode control for systems with mismatched disturbances', *Automatica*, 2013, **49**, (7), pp. 2287–2291

[20] Xu, Q., Cao, Z.: 'Piezoelectric positioning control with output-based discrete-time terminal sliding mode control', *IET Control Theory Appl.*, 2017, **11**, (5), pp. 694–702

[21] Silva, J.M.A.D., Edwards, C., Spurgeon, S.K.: 'Sliding-mode output feedback control based on LMIs for plants with mismatched uncertainties', *IEEE Trans. Ind. Electron.*, 2009, **56**, (9), pp. 3675–3683

[22] Zhang, J., Xia, Y.: 'Design of static output feedback sliding mode control for uncertain linear systems', *IEEE Trans. Ind. Electron.*, 2010, **57**, (6), pp. 2161–2170

[23] Park, P.G., Choi, D.J., Kong, S.G.: 'Output feedback variable structure control for linear systems with uncertainties and disturbances', *Automatica*, 2007, **43**, (1), pp. 72–79

[24] Choi, H.H.: 'Sliding-mode output feedback control design', *IEEE Trans. Ind. Electron.*, 2008, **55**, (11), pp. 4047–4054

[25] Cunha, J.P.V.S., Costa, R.R., Lizarralde, F.*, et al.*: 'Peaking free variable structure control of uncertain linear systems based on a high-gain observer', *Automatica*, 2009, **45**, pp. 1156–1164

[26] Daly, J.M., Wang, D.W.L.: 'Output feedback sliding mode control in the presence of unknown disturbances', *Syst. Control Lett.*, 2009, **58**, (3), pp. 188–193

[27] Basin, M.V., Panathula, C.B., Shtessel, Y.B.*, et al.*: 'Continuous finite-time higher order output regulators for systems with unmatched unbounded disturbances', *IEEE Trans. Ind. Electron.*, 2016, **63**, (8), pp. 5036–5043

[28] Xia, Y., Fan, P., Fu, M.*, et al.*: 'Modeling and compound control for unmanned turret system with coupling', *IEEE Trans. Ind. Electron.*, 2016, **63**, (9), pp. 5794–5803

[29] Li, S., Wu, C., Sun, Z.: 'Design and implementation of clutch control for automotive transmissions using terminal-sliding-mode control and uncertainty observer', *IEEE Trans. Veh. Technol.*, 2016, **65**, (4), pp. 1890–1898

[30] Han, J.: 'From PID to active disturbance rejection control', *IEEE Trans. Ind. Electron.*, 2009, **56**, (3), pp. 900–906

[31] Guo, B., Zhao, Z.: 'On convergence of non-linear extended state observer for multi-input multi-output systems with uncertainty', *IET Control Theory Appl.*, 2012, **6**, (15), pp. 2375–2386

[32] Talole, S.E., Kolhe, J.P., Phadke, S.B.: 'Extended-state-observer-based control of flexible-joint system with experimental validation', *IEEE Trans. Ind. Electron.*, 2010, **57**, (4), pp. 1411–1419

[33] Xia, Y., Zhu, Z., Fu, M.: 'Back-stepping sliding mode control for missile systems based on an extended state observer', *IET Control Theory Appl.*, 2011, **5**, (1), pp. 93–102

[34] Wang, J., Li, S., Yang, J.*, et al.*: 'Extended state observer-based sliding mode control for PWM-based DC–DC buck power converter systems with mismatched disturbances', *IET Control Theory Appl.*, 2015, **9**, (4), pp. 579–586

[35] Godbole, A.A., Kolhe, J.P., Talole, S.E.: 'Performance analysis of generalized extended state observer in tackling sinusoidal disturbances', *IEEE Trans. Control Syst. Technol.*, 2013, **21**, (6), pp. 2212–2223

[36] Kim, W., Choo, C.C.: 'Robust output feedback control for unknown non-linear systems with external disturbance', *IET Control Theory Appl.*, 2016, **10**, (2), pp. 173–182

[37] Sira-Ramírez, H., Oliver-Salazar, M.A.: 'On the robust control of buck-converter DC-motor combinations', *IEEE Trans. Power Electron.*, 2013, **28**, (8), pp. 3912–3922

[38] Guo, B., Zhao, Z.: 'On the convergence of an extended state observer for nonlinear systems with uncertainty', *Syst. Control Lett.*, 2011, **60**, (6), pp. 420–430

[39] Kim, K.S., Rew, K.H., Kim, S.: 'Disturbance observer for estimating higher order disturbances in time series expansion', *IEEE Trans. Autom. Control*, 2010, **55**, (8), pp. 1905–1911

[40] Khalil, H.K.: '*Nonlinear systems*' (Prentice-Hall, New Jersey, 2002, 3rd edn.)

[41] Yu, S., Yu, X., Shirinzadeh, B.*, et al.*: 'Continuous finite-time control for robotic manipulators with terminal sliding mode', *Automatica*, 2005, **41**, (11), pp. 1957–1964